ANNALS of Clinical and Translational Neurology
Open Access
ANA American Neurological Association since 1875

RESEARCH ARTICLE

Deep sequencing of mitochondrial genomes reveals increased mutation load in Friedreich's ataxia

Angela D. Bhalla[1], Alireza Khodadadi-Jamayran[1], Yanjie Li[1], David R. Lynch[2] & Marek Napierala[1,3,]

[1]Department of Biochemistry and Molecular Genetics, University of Alabama at Birmingham, UAB Stem Cell Institute, 1825 University Blvd., Birmingham, Alabama 35294
[2]Division of Neurology and Pediatrics, Children's Hospital of Philadelphia, Abramson Research Center, Room 502, Philadelphia, Pennsylvania 19104
[3]Department of Molecular Biomedicine, Institute of Bioorganic Chemistry, Polish Academy of Sciences, Poznan 61-704, Poland

Correspondence
Marek Napierala, University of Alabama at Birmingham, Department of Biochemistry and Molecular Genetics, UAB Stem Cell Institute, 1825 University Blvd., Birmingham, AL 35294. Tel: 205 975 5320; Fax: 205 975 3335; E-mail: mnapiera@uab.edu

Funding Information
This study was supported by the National Institute of Health (7R01NS081366) from NINDS to M. N., a Muscular Dystrophy Association grant (MDA0789 to M. N.), a Friedreich's Ataxia Research Alliance, and FARA Ireland grant to M. N., and a National Ataxia Foundation Postdoctoral Fellowship to A. D. B.

Received: 10 May 2016; Accepted: 12 May 2016

Annals of Clinical and Translational Neurology **2016; 3(7): 523–536**

doi: 10.1002/acn3.322

Abstract

Objective: Friedreich's ataxia (FRDA) is an autosomal recessive trinucleotide repeat expansion disorder caused by epigenetic silencing of the frataxin gene (*FXN*). Current research suggests that damage and variation of mitochondrial DNA (mtDNA) contribute to the molecular pathogenesis of FRDA. We sought to establish the extent of the mutation burden across the mitochondrial genome in FRDA cells and investigate the molecular mechanisms connecting *FXN* downregulation and the acquisition of mtDNA damage. **Methods**: Damage and mutation load in mtDNA of a panel of FRDA and control fibroblasts were determined using qPCR and next-generation MiSeq sequencing, respectively. The capacity of FRDA and control cells to repair oxidative lesions in their mtDNA was measured using a quantitative DNA damage assay. Comprehensive RNA sequencing gene expression analyses were conducted to assess the status of DNA repair and metabolism genes in FRDA cells. **Results**: Acute or prolonged downregulation of *FXN* expression resulted in a significant increase in mtDNA damage that translated to a significant elevation of mutation load in mtDNA. The predominant mutations identified throughout the mtDNA were C>T, G>A transitions ($P = 0.007$). Low *FXN* expression reduced capacity to repair oxidative damage in mtDNA. Downregulation of *FXN* expression strongly correlated ($r = 0.73$) with decreased levels of base excision repair (BER) DNA glycosylase *NTHL1*. **Interpretation**: Downregulation of *FXN* expression in FRDA cells elevates mtDNA damage, increases mutation load of the mitochondrial genome, and diminishes DNA repair capacity. Progressive accumulation of mtDNA mutations in vulnerable FRDA patient cells reduces mitochondrial fitness ultimately leading to cell death.

Introduction

Friedreich's ataxia (FRDA) is an autosomal recessive neurodegenerative disorder affecting approximately 1 in 50,000 individuals. FRDA is characterized by degeneration of dorsal root ganglion sensory neurons and spinocerebellar tracts, cardiomyopathy, diabetes, and hearing loss among other features[1,2] and is caused by insufficient levels of frataxin (FXN), a nuclear-encoded mitochondrial protein[3]. Transcriptional repression of *FXN* mRNA expression in FRDA results from an expansion of the guanine–adenine–adenine (GAA) trinucleotide repeat tract in the first intron of the *FXN* gene from 6–34 repeats in unaffected individuals to 66–1500 repeats in FRDA patients[1, 4]. The exact molecular role of frataxin is yet to be experimentally proven, but a general consensus exists that this small iron-binding protein functions at the cross-roads of several pathways regulating iron metabolism[5]. Results of current research indicate that FXN acts as an iron chaperone critical for biosynthesis of iron–sulfur clusters (ISCs) and heme, or as a molecular switch between the ISC and heme synthesis pathways[5]. Since

ISCs are critical prosthetic groups of various cellular proteins, pleiotropic effects of frataxin deficiency can be, at least in part, attributed to defects in ISC biosynthesis[6]. In addition, several studies implicated a protective role for frataxin against reactive oxygen species (ROS)-mediated oxidative stress[7–9]. Lastly, potential functions of FXN as an iron storage molecule or an iron sensor have been proposed based predominantly on analyses conducted in bacteria and lower eukaryotes[5].

FRDA is characterized by a pronounced deficit of mitochondrial function. Decreased FXN levels impair adenosine triphosphate (ATP) production and aconitase activity[10,11]. In addition, mitochondrial iron overload is observed in yeast and mouse FRDA models as well as in patient tissues[12–14]. Low FXN levels lead to increased ROS production and increased ROS sensitivity in yeast, FRDA patient-derived fibroblasts and lymphoblasts, and other tissues[7–9]. ROS, byproducts of normal cellular metabolism, can cause many different types of DNA lesions[15]. Excessive ROS levels can be detrimental to the cell by damaging mitochondrial DNA (mtDNA), which can impair the function of mitochondrial proteins including electron transport chain (ETC) complexes, resulting in even greater ROS production[15,16]. Although elevated levels of ROS have been detected in FRDA cells, the potential effect of FXN deficiency on DNA mutations and genome stability in FRDA remains unclear.

Increased levels of mtDNA damage are an established hallmark of many neurodegenerative diseases including Alzheimer's disease and Huntington's disease[17]. The link between FXN deficiency and elevated mtDNA damage was first demonstrated in yeast lacking Yfh1 (the yeast homolog of *FXN*)[18]. Human peripheral blood cells isolated from FRDA-affected individuals also exhibit increased nuclear and mtDNA damage[19].

It has been postulated that the mtDNA sequence variation observed in FRDA contributes to its progressive degenerative disease phenotype[20–22]. Indeed, a greater number of mtDNA deletions and heteroplasmic variations were identified in an Iranian FRDA cohort than in controls using conventional sequencing[20]. The number of mitochondrial displacement loop (D-loop) variants positively correlated with the length of the shorter GAA allele (GAA1), hence inversely correlated with *FXN* expression[21]. Additionally, targeted resequencing of the mitochondrial D-loop, mitochondrially encoded NADH dehydrogenase genes (MT-ND), and ATP synthase genes (MT-ATP6, MT-ATP8) in a North Indian FRDA population showed increased mtDNA variation and suggested nonsynonymous variation in both the Complex I and ATP genes involved in disease pathogenesis[22].

The aforementioned studies used conventional sequencing and targeted resequencing approaches which provided informative snapshots of mtDNA sequence variation at specific locations. In this study, we employed a high-throughput next-generation sequencing technique which enabled us to examine the consequences of FXN deficiency on the stability of the entire 16.5 kbp mitochondrial genome. Given the relatively small size of the mtDNA, our high-throughput approach successfully sequenced every nucleotide in the mitochondrial genome at an average of over 16,000 times for each cell line. The volume of sequences generated by this approach allowed for robust analysis of the mutational landscape of mtDNA from FRDA and control cells.

Herein, we demonstrate using next-generation DNA sequencing approaches that *FXN* deficiency results in an increased frequency of mtDNA mutations. The level of *FXN* expression correlated with mutation load as well as with expression of the BER DNA glycosylase *NTHL1* (Nth Endonuclease III-Like 1). We propose that accumulation of mtDNA lesions represents a critical event in the development and progression of FRDA.

Materials and Methods

Cell culture

Primary fibroblasts were cultured in Dulbecco's Modified Eagle Medium (DMEM; Life Technologies, Carlsbad, CA) supplemented with 15% fetal bovine serum (Hyclone, GE, Pittsburgh, PA), 1 × non-essential amino acids (Life Technologies), and 2 mmol/L GlutaMAX (Life Technologies). Lentiviruses were generated by co-transfecting 293T cells using Lipofectamine 2000 (Life Technologies) with either control or FXN short hairpin RNA constructs (FXN: TRC Human FXN shRNA Clone ID TRCN0000006137 and TRCN0000006138, Dharmacon; control: SHC002, Sigma-Aldrich, St Loius, MO), along with psPAX2 and pMD2.G (Addgene, Cambridge, MA) vectors. Virus-containing medium was collected at 48 h, 60 h, and 72 h after transfection, and filtered with 0.45 μm filter. Fibroblasts were transduced with lentivirus for 24 h at 37°C in the presence of 5 μg/mL polybrene. Cells were then maintained in complete DMEM supplemented with 5 μg/mL puromycin (Calbiochem, EMD Millipore, Germany) for 6 days before harvesting. Human-induced pluripotent stem cells (hiPSCs) were cultured in mTeSR-1 (Stem Cell Technologies, Vancouver, BC, Canada), on plates coated with Matrigel (Corning, Corning, NY) with enzymatic passaging using dispase (Stem Cell Technologies) as previously described[23]. hiPSCs stably transduced with FXN or control lentiviral shRNAs were maintained in mTeSR-1 medium containing 1 μg/mL puromycin.

PCR analyses

MtDNA damage assay

Mitochondrial DNA damage was determined by quantitative PCR (qPCR) as described[24]. Briefly, total DNA was isolated using the GenElute™ Mammalian Genomic DNA Miniprep Kit, (Sigma-Aldrich) and quantitated as described[24]. The long ~9.5 kbp mtDNA qPCR product was amplified in a 50 μL volume using 15 ng of total DNA template and quantitated as described[24]. Quantitative PCR using 3 ng of DNA template in a 10 μL volume was used for amplification of the ~0.2 kbp short mtDNA fragment using Power SYBR® Green PCR Master Mix (Life Technologies) as follows: 95°C, 10 min; 40 cycles of: 95°C, 15 sec, 60°C, 30 sec. The short mtDNA product was quantitated using the $2^{-\Delta\Delta CT}$ method. Relative amplification was determined by normalizing the long mtDNA PCR product to the short mtDNA PCR product[24].

mtDNA copy number

Total DNA was isolated as above, then quantitation of mtDNA copy number was performed by qPCR[25] using short mtDNA primers to measure mtDNA content and Control 3 primers to measure nuclear DNA. The Control 3 primer set hybridizes to a nonredundant intergenic region on chromosome 17. Primer sequences are presented in Table 1.

Quantitative reverse transcriptase PCR

Quantitative RT-PCR was performed as described[23]. Briefly, total RNA was isolated using the RNeasy Mini Kit (Qiagen, Valencia, CA) and DNase-treated with the TURBO DNA-free kit (Life Technologies). The qRT-PCR reactions were performed using Power SYBR Green RNA-to-CT 1-Step Kit (Life Technologies) with the following PCR conditions: reverse transcription, 48°C for 30 min; 40 cycles of 95°C, 15 sec, 60°C, 1 min. Reactions without reverse transcriptase were included to verify the absence of genomic DNA. mRNA expression was normalized to *GAPDH* mRNA. Relative expression was determined using the $2^{-\Delta\Delta CT}$ method. Primer sequences are presented in Table 1.

GAA repeat length analysis

GAA repeat PCR was performed using the FXN_long primer set, which amplifies the GAA repeat tract and 1370 bp of flanking sequences, as described[23]. Briefly, 50–100 ng of genomic DNA was amplified with the Failsafe PCR system and mix D (Epicentre, Madison, WI). PCR products were visualized on 1% agarose gels. Primer sequences are presented in Table 1.

MiSeq mtDNA sequencing

Mitochondrial DNA was amplified as two overlapping ~9 kbp and ~11 kbp fragments with MTL1 and MTL2 primer sets, respectively[26]. PCR reactions were performed in a 50 μL volume using 1 ng of template DNA as follows: 94°C, 5 min; 98°C, 15 sec; 68°C, 10 sec; (slow ramp from 68°C to 60°C at 0.2°C per sec); 60°C, 15 sec; 68 °C, 11 min for 30 cycles to assure that reactions terminated in the exponential phase, followed by terminal elongation at 72°C, 10 min. A quantity of 1 μg of PCR product, obtained by combining the ~9 kbp and ~11 kbp fragments in equimolar ratio, was sequenced at the UAB Heflin Center for Genomic Science using an Illumina MiSeq Desktop Sequencer (Illumina, San Diego CA). Libraries were prepared using a TruSeq DNA PCR-Free Library Preparation kit according to manufacturer's instructions (Illumina), and sequenced using the MiSeqv2 kit (Illumina).

Bioinformatic analyses

We obtained an average of 1.3 million paired-end reads (251 × 2) for all samples. Reads for each sample were

Table 1. Primers used in this study.

Gene	Forward 5′–3′	Reverse 5′–3′	Amplicon
Long mtDNA	TCTAAGCCTCCTTATTCGAGCCGA	TTTCATCATGCGGAGATGTTGGATGG	8843
Short mtDNA	CCCCACAAACCCCATTACTAAACCCA	TTTCATCATGCGGAGATGTTGGATGG	222
FXN_long	GGAGGGAACCGTCTGGGCAAAGG	CAATCCAGGACAGTCAGGGCTTT	Varies
Control 3	GAGTGGGATTCCCCCAGAATG	AAGTGCAAAGTCGGTGGTGA	81
FXN	CAGAGGAAACGCTGGACTCT	AGCCAGATTTGCTTGTTTGG	172
GAPDH	GAAGGTGAAGGTCGGAGTC	GAAGATGGTGATGGGATTTC	226
MTL1	AAAGCACATACCAAGGCCAC	TTGGCTCTCCTTGCAAAGTT	9065
MTL2	TATCCGCCATCCCATACATT	AATGTTGAGCCGTAGATGCC	11171
NTHL1_b	GGGCACTGTGTCAGGCATT	GGACTTGGTTGCCTTCTTGGT	85

mapped to the mitochondrial reference genome (rCRS NC_012920.1) using the BWA (v0.7.5a) mem algorithm[27]. Duplicate reads were removed using Picard-tools (v1.100) (http://picard.sourceforge.net). Indel realignment was performed using the Genome Analysis Toolkit (GATK, v2.7–2, Broad Institute, Cambridge, MA)[28]. Reads with low mapping quality (MQ < 30) were removed from the analysis. The number of all possible bases (A, T, C, G) for each position were counted using GATK's "DepthOfCoverage" tool (bases with low quality [Q < 30] were discounted) and NGSUtils's (v0.5.7) "basecall" tool was used to count the number of insertions and deletions at each position. The variants excluded from the analysis were 333 variants with a minor allele frequency >0.01 for all populations submitted to the database of short genetic variations (NCBI dbSNP Build 141, http://www.ncbi.nlm.nih.gov/SNP/index.html) and the mitochondrial DNA hypervariable regions (mtDNA positions 16,024–576). To increase the accuracy of the analysis, a consensus reference sequence was made based on the most abundant base at each position for each sample to obtain a sample-specific mismatch table (including indels). Mismatch tables were normalized by each sample's library size factor using DESeq (v3.0)[29]. Differential mutation/mismatch rate analysis was performed in DESeq and mutation hot spots were identified (≥1.5 fold change). The averages of the mutation frequencies in controls and patients were compared using student's *t*-test. Statistical analyses and plotting were performed in R (v3.1.1, http://www.r-project.org/).

DNA damage induction

Ten centimeter dishes were seeded with primary FRDA and control fibroblasts 24 h prior to treatment with 200 μmol/L H_2O_2 (ThermoFisher, Grand Island, NY) for 15 min and harvested immediately or allowed to recover for 3 or 12 h. Total DNA was isolated and mtDNA damage was analyzed as described above.

RNA sequencing analysis

RNA sequencing for 17 control fibroblast lines and 18 FRDA fibroblast lines was conducted as described in[30]. Briefly, libraries were prepared using the TruseqStranded Total RNA Sample Prep kit (Illumina), which includes a step for depletion of ribosomal RNA. Sequencing was performed using HiSeq2000 (Illumina), with a protocol that generated 2 × 76 bases paired-end reads. Following mapping and filtering of poor-quality reads, differential expression was determined using DESeq (version 1.10.1). Pearson's correlation of *NTLH1* expression with *FXN* expression was calculated in GraphPad Prism 6.

Statistical analyses

Statistical analyses were conducted using GraphPad Prism 6, unless described otherwise. Statistical significance was determined by two-tailed Student's *t*-test, $P < 0.05$ was considered significant.

Results

Increased mtDNA damage in FRDA primary fibroblasts

To investigate the effect of FXN deficiency on mtDNA damage in a representative group of five control and five primary FRDA fibroblast lines derived from skin biopsies in our laboratory[31](Table 2), we employed an established PCR method for quantification of mtDNA damage[24]. First, we verified the GAA trinucleotide repeat length and *FXN* mRNA expression in our fibroblast cohort by PCR, and quantitative reverse transcriptase PCR (qRT-PCR), respectively (Fig. 1A–B). All five FRDA lines carried GAA repeat expansions, while the control lines did not harbor any expansions indicating that no heterozygous, asymptomatic carriers were included in the control cohort. As expected, the qRT-PCR analysis showed that the FRDA lines expressed lower levels of *FXN* mRNA relative to the average *FXN* mRNA expression in control lines. Next, we sought to determine the extent of mtDNA damage in FRDA and control cells. The mtDNA damage qPCR method used is based on the principle that DNA carrying lesions is amplified less efficiently than DNA without lesions; thus, an inverse relationship exists between the frequency of DNA lesions and the amount of PCR product. Briefly, a long mtDNA fragment (8843 bp) and a short mtDNA fragment (222 bp) were amplified from total DNA isolated from primary fibroblasts at the time of derivation from skin biopsies[31] (Fig. 1C, left panel). Thus, material for these experiments was isolated before any of the lines reached passage 5. The amount of long

Table 2. Gender, sampling age, and GAA repeat expansion size for primary fibroblast lines used in this study.

Sample	Gender	Age at sampling (years)	GAA repeat length
C1	F	19	Unaffected
C2	F	11	Unaffected
C3	M	52	Unaffected
C4	F	27	Unaffected
C5	M	10	Unaffected
F1	F	21	576, 1043
F2	F	44	526, 826
F3	F	50	422, 520
F4	M	29	500, 1043
F5	M	19	643, 806

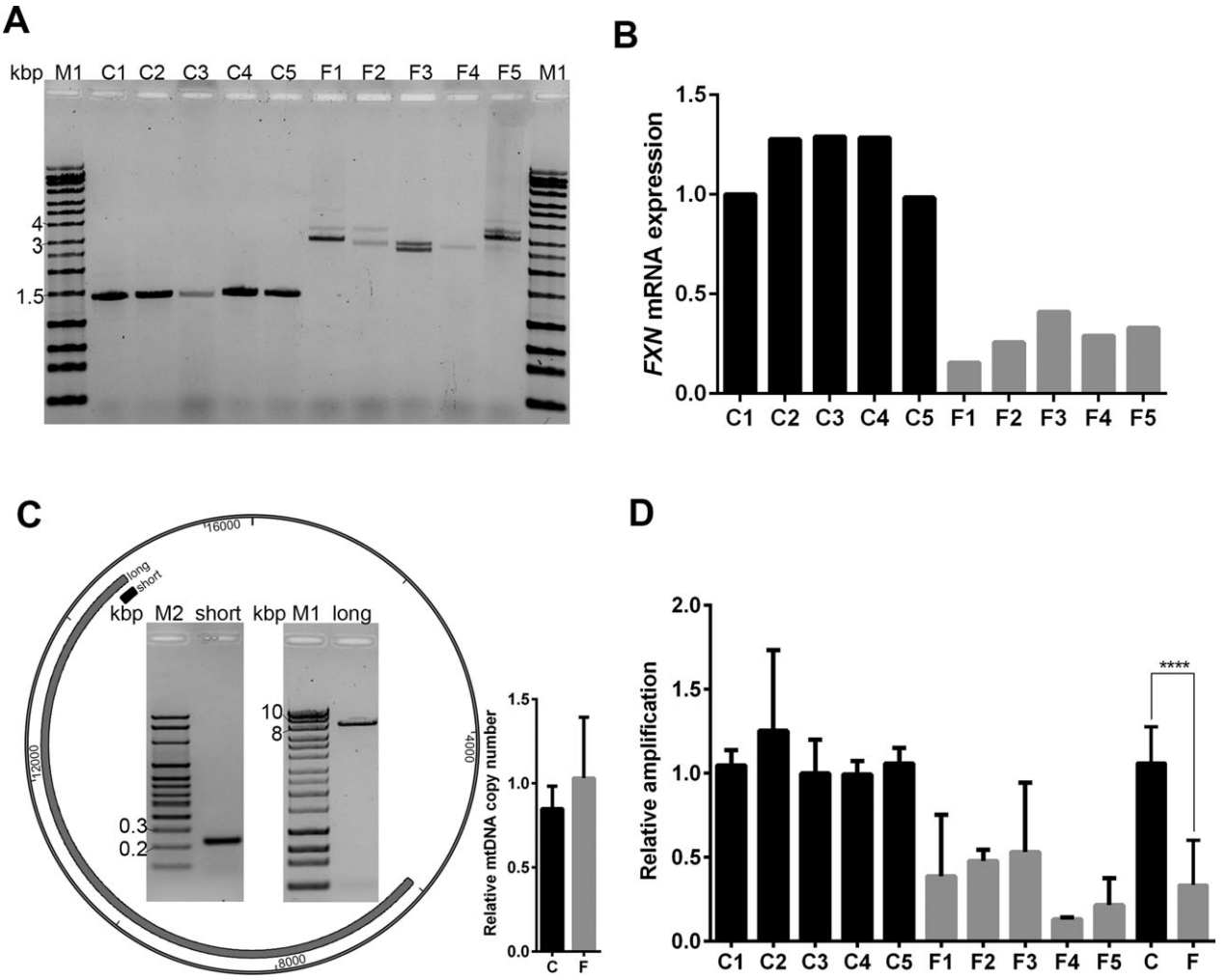

Figure 1. Increased mtDNA damage in FRDA fibroblasts. (A) PCR analysis of GAA repeat length in FRDA and control fibroblasts; M1 = HyperLadder Plus 1 kbp ladder, C1–C5 = controls, F1–F5 = FRDA. (B) qRT-PCR analysis of *FXN* mRNA expression in fibroblast lines used in this study; C1–C5 shown in black, F1–F5 shown in gray. *FXN* expression was normalized to *GAPDH* mRNA level. (C) Left panel: Representative agarose gel electrophoresis and amplicons for mtDNA damage qPCR products; M1 = HyperLadder™ 1 kb Plus ladder (catalog # BIO-33068, Bioline, Taunton, MA); M2 = HyperLadder™ 100 bp Plus ladder (catalog # BIO-33071, Bioline); long = long PCR product, ~8.8 kbp; short = short PCR product, 222 bp. Long amplicon shown in gray, short amplicon shown in black. Right panel: qPCR analysis of mtDNA copy number in control (C) and FRDA (F) fibroblasts. Results shown are from two independent experiments with five biological replicates for each group. (D) mtDNA damage qPCR analyses of short and long fragments were performed for control and FRDA fibroblasts; results from at least three independent experiments are shown. Controls (C1–C5) are depicted in black and FRDA (F1–F5) are depicted in gray. Cumulative analysis of the data for entire C and F cohort is shown; **** indicates $P < 0.0001$.

PCR product was normalized to mtDNA copy number using the relative amount of the short mtDNA fragment amplified by qPCR. The FRDA fibroblast lines assayed for mtDNA damage showed a significant increase in mtDNA damage compared to control fibroblasts (Fig. 1D). In addition to mtDNA copy number normalization using the short mtDNA PCR fragment (Fig. 1C, left panel), we independently assessed the possibility of mtDNA depletion in FRDA fibroblasts by quantifying its amount relative to a nonredundant intergenic region of nuclear DNA located on chromosome 17 (Fig. 1C, right panel). No statistically significant differences in mtDNA content were detected between FRDA and control fibroblasts (Fig. 1C, right panel). In summary, these results demonstrate that FRDA fibroblasts exhibit a higher level of mtDNA damage compared to unaffected cells.

Rapid FXN depletion elicits mtDNA damage in control cells

To determine whether *FXN* expression level is directly linked to the level of mtDNA damage observed in FRDA

cells, *FXN* mRNA was depleted by lentiviral-mediated transduction of two different short hairpin RNAs (shRNAs) specific for *FXN* mRNA in C1 primary fibroblasts for a duration of 6 days. The extent of mtDNA damage was quantitated using the qPCR method described in Figure 1D. The relative amplification of mtDNA was decreased by approximately 50% using two different shRNAs against *FXN* (Fig. 2A) indicating an elevated level of DNA damage. The level of *FXN* mRNA expression was reduced to ~10–30% of the *FXN* mRNA level in control fibroblasts transduced with a nontargeting, control shRNA (Fig. 2B). Similar results were observed in human induced-pluripotent stem cells (hiPSCs) stably expressing control or *FXN* shRNAs (Fig. 2C). This result demonstrated that control cells, depleted of FXN, acquire mtDNA damage in a manner similar to the constitutive downregulation of *FXN* typical for FRDA patient cells.

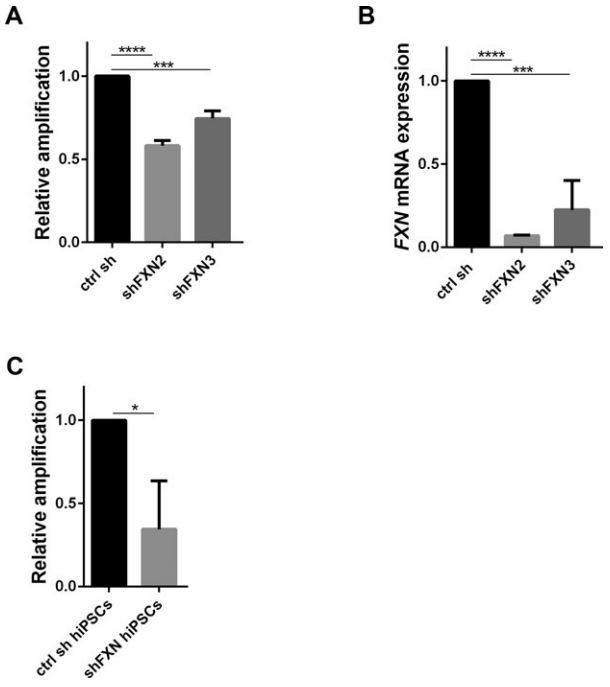

Figure 2. *FXN* depletion causes mtDNA damage in control cells. (A) Quantitation of mtDNA damage after 6 days of *FXN* depletion, displayed as relative amplification of long mtDNA PCR product normalized to short mtDNA PCR product for frataxin-depleted C1 fibroblasts; Ctrl sh indicates nontargeting shRNA; shFXN2 and shFXN3 denotes two different *FXN*-specific shRNAs. (B) Quantitation of lentiviral-mediated shRNA depletion of *FXN* in C1 fibroblasts after 6 days of *FXN* depletion. (C) Quantitation of mtDNA damage in *FXN* depleted hiPSC lines stably depleted of *FXN* mRNA. Results of three independent experiments are shown; ****$P = 0.0001$, ***$P = 0.001$ and *$P = 0.02$.

Mitochondrial DNA mutation frequency is increased in FRDA fibroblasts

Higher levels of mtDNA damage detected in FRDA cells (Fig. 1), if not corrected by efficient repair mechanisms, may translate into an increased mutation load. To determine the extent of mtDNA mutations across the entire mitochondrial genome, we performed high-throughput sequencing of the mitochondrial genomes in the same panel of fibroblasts used to analyze mtDNA damage (Table 2). We amplified the entire mitochondrial genome in two overlapping fragments, ~9 kb and ~11 kb[26] (Fig. 3A). The PCR fragments, amplified to early exponential phase, were combined in equimolar ratios and sequenced using the Illumina MiSeq sequencer. Sequencing reads were aligned to the revised Cambridge Reference Sequence (rCRS)[32]. The high sequencing coverage (mean coverage of 16,047× per base) allowed for an in-depth analysis of mtDNA mutation load in FRDA and control fibroblasts. We accounted for mtDNA variation that might arise from differences in mitochondrial haplotype in individual samples by creating a consensus mitochondrial genome for each sample in which the nucleotide occurring most frequently at each mtDNA position was considered the reference for that individual's genome (see Material and Methods). Mutations were identified by creating mismatch tables and mutation frequencies were determined as the number of times a non-reference base was called at each position. The mutation frequencies were normalized by each samples library size factor. Transitions (a purine–purine or pyrimidine–pyrimidine mutation), transversions (a purine–pyrimidine or pyrimidine–purine mutation), insertions and deletions (indels) rates were also calculated after normalization. Combined analyses of all FRDA and control cells demonstrated that the overall mutation frequency in FRDA fibroblasts (blue bar) is significantly increased compared to control fibroblasts (red bar), (Fig. 3B). There was no overlap in the mutation frequency for any control sample into the FRDA group or vice versa, signifying that the increased mutation frequency is a distinct characteristic of the FRDA population (Fig. 3C). We detected a significant inverse correlation ($r = -0.70$) between mutation frequency and *FXN* expression (Fig. 3D). The mtDNA mutation frequency, shown as an area plot, is increased across the entire genome in FRDA fibroblasts (blue) compared to controls (red; Fig. 3E). To prevent regions with known high mutation frequency in from masking mtDNA mutation frequency, the control region of the mitochondrial genome (positions 16024–576) containing the D-loop and hypervariable segments I and II (mtDNA positions 16024–16383 and 57–372, respectively[33]) were

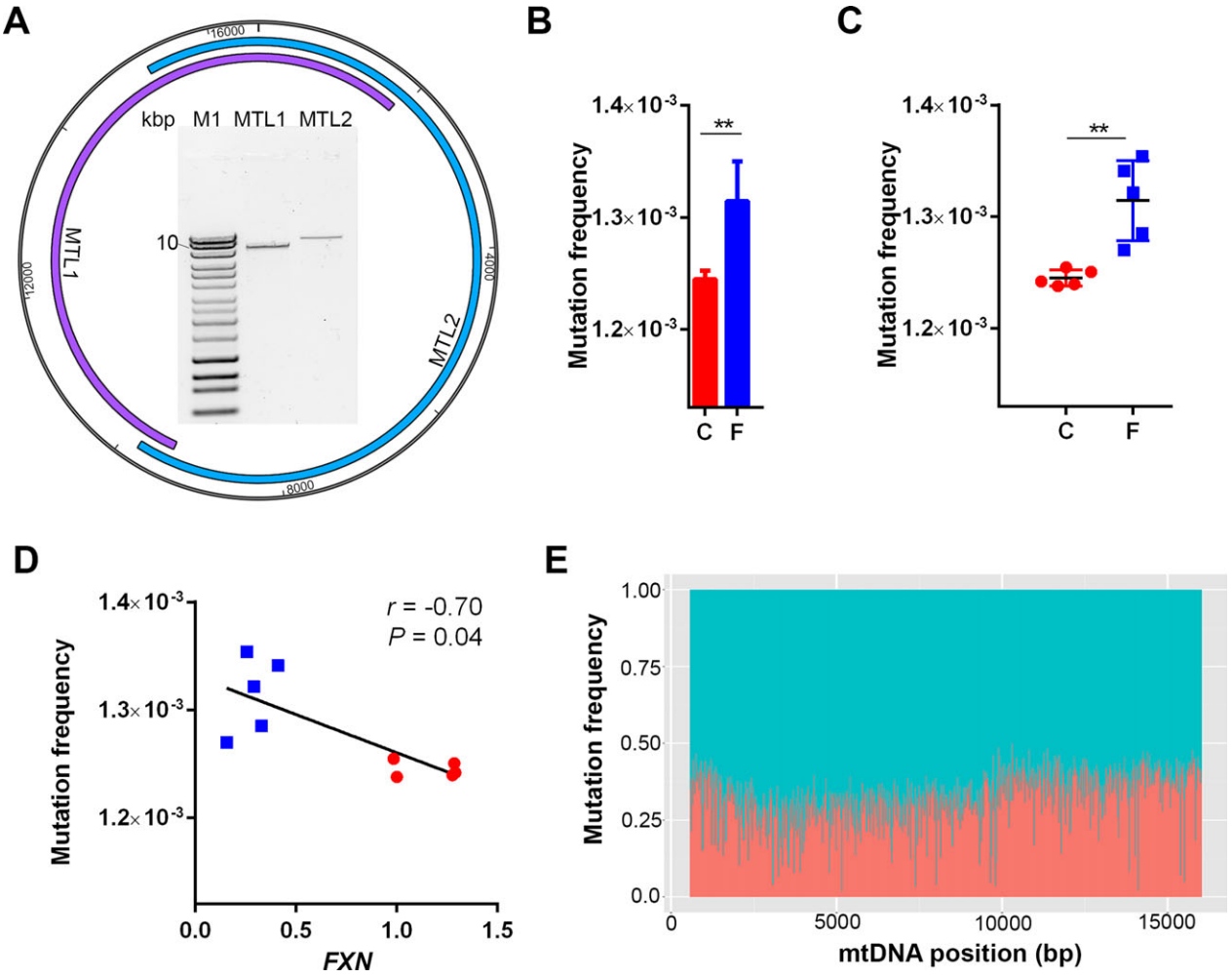

Figure 3. Mitochondrial DNA mutation frequency is increased in FRDA fibroblasts. (A) Schematic amplicons and representative agarose gel electrophoresis analysis of PCR products used in MiSeq sequencing of the mtDNA. M1 = HyperLadder™ 1 kb Plus ladder, MTL1 = ~9 kbp, MTL2 = ~11 kbp. (B) Quantitation of cumulative mtDNA mutation frequency, respectively, for C (red bar) and F (blue bar) cohorts, $^{**}P = 0.003$. (C) Quantitation of mtDNA mutation frequency in individual C1–C5 samples (red circles) and F1–F5 samples (blue squares); $^{**}P = 0.003$. (D) Correlation between mutation frequency and *FXN* expression determined by RNAs-seq signal for C1–C5 (red circles), F1–3, F5 (blue squares). Pearson's correlation coefficient (r) and statistical significance (P) values are indicated on the graph. (E) Mutation frequency depicted as an area plot for control (shown in red) and FRDA (shown in blue) fibroblasts. The X-axis shows individual positions in mtDNA; the region spanning mtDNA from position 16,024 to 576 (total of 1122 bp) containing two hypervariable segments has been excluded from analyses. Mutation frequency was calculated by normalizing the number of mutations (transitions, transversions, and single-nucleotide indels) to the library size factor for each sample. On the Y-axis, 1 represents a combined total number of mutations identified at each position of the mtDNA in both C and F cohorts. The blue area represents the fraction of total mutations identified in FRDA cells while red depicts the fraction of total mutations identified in control fibroblasts.

excluded from the analyses. To determine whether the increased mutation load observed in FRDA cells is distributed evenly across the genome or concentrated at certain positions, we calculated the fold change of the mutation frequency for each mtDNA position after removal of the control region. Analyses revealed 2364 residues in mtDNA from FRDA cells exhibited ≥1.5-fold frequency of mutation when compared to their counterpart residues in mtDNA of control fibroblasts. Fourteen residues were identified as "hotspots" for mutations, with an 11–54-fold increase in mutation frequency relative to the corresponding residues in controls. Taken together, our results from high-throughput next-generation sequencing of mitochondrial genomes demonstrated that FRDA cells carry a significantly higher mutation load than controls.

Transition frequency is elevated in mtDNA of FRDA fibroblasts

As the types of mutations occurring in FRDA cells could provide insights into specific DNA repair defects that may be involved in disease progression, we determined the mtDNA mutation spectra (transitions, transversions, and indels) for FRDA and control fibroblasts. Importantly, the transition frequency was significantly increased in FRDA fibroblasts compared to control cells (Fig. 4A). Inspection of the classes of transitions indicated that in particular, [A>G, T>C] transitions occur roughly fourfold more frequently than [G>A, C>T] in both control and FRDA populations, however, there was a significant increase in [C>T, G>A] transitions in FRDA cells (Fig. 4B). In contrast, there was no overrepresentation of any class of transversions in FRDA cells (Fig. 4B). The frequency of each class of transversions was similar in control and

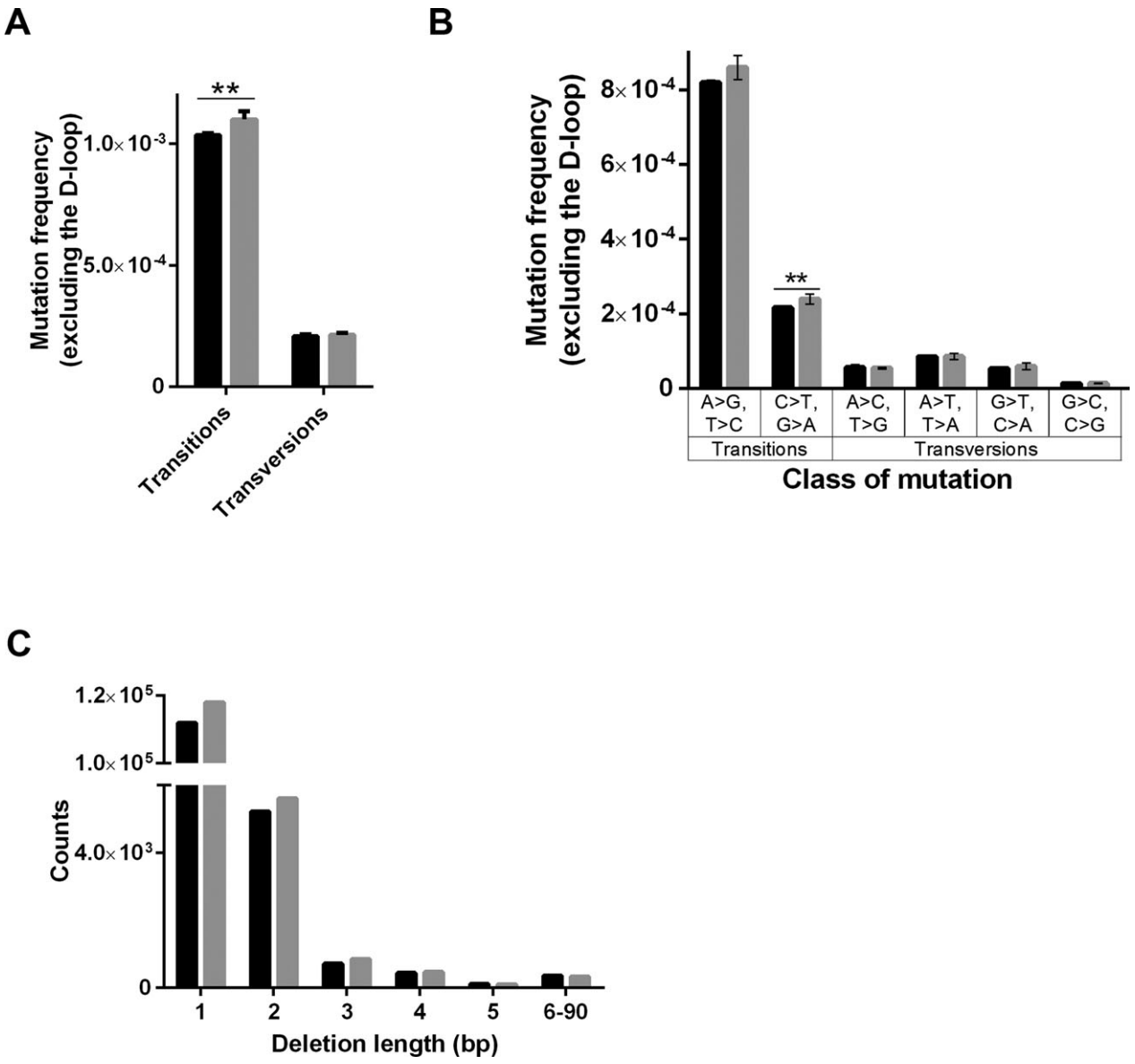

Figure 4. Frequency of substitutions and deletions in FRDA and control fibroblasts. (A) Transition and transversion frequency in controls (shown in black), and FRDA cells (shown in gray), $^{**}P = 0.004$. Mutation frequencies were calculated by normalizing the number of mutated bases to the number of wild-type bases. (B) Frequency of transitions and transversions classes in FRDA (gray bars) and control (black bars) fibroblasts; $^{**}P = 0.007$. (C) Total count of mono-, di-, tri-, tetra-, penta-nucleotide as well as larger (6–90 bp) deletions in control (shown in black) and FRDA (shown in gray) samples. The total number of deletions was normalized to the library size factor.

FRDA samples, and of the four classes, [G>C, C>G] were the most rarely observed (Fig. 4B). In general, in the nuclear DNA of most species studied, transitions occur more frequently than transversions[34]. The transition: transversion (T_i/T_v) ratio in mtDNA is typically higher than the expected 1:2 proportion based on assumption of equal probability of all substitutions[34]. In agreement with previous studies, we observed a T_i/T_v of 4.98 and 5.15 for control and FRDA mtDNA, respectively. The frequency of deletions encompassing 1–90 bp did not increase significantly in FRDA cells; however, FRDA cells exhibited a higher frequency of small, 1–3 bp deletions in the mtDNA (Fig. 4C). Overall, the most prominent were single base pair deletions, comprising over 94% of the total number of deletions in both control and FRDA cells. In conclusion, these results showed a significantly higher frequency of transitions in mtDNA of FRDA fibroblasts and similar frequency of transversions in both control and FRDA cohorts. A trend indicating elevated frequency of small deletions was also detected in FRDA cells.

FRDA primary fibroblasts have decreased mtDNA repair capacity

To investigate further the response to mtDNA damage in our human primary fibroblast model system, we determined the ability of FRDA cells to recover from oxidative mtDNA damage. It has been previously reported that FXN overexpression in Chinese hamster V79 fibroblasts reduced the basal level of oxidative DNA damage[35]. Given the greater amount of mtDNA mutations observed in FRDA fibroblasts (Fig. 3), we considered the possibility of reduced mtDNA repair capacity in FRDA cells. Oxidative DNA damage was induced by treatment of C1 and F1 fibroblasts with 200 μmol/L H_2O_2 for 15 min, and cells were immediately harvested or allowed to recover for 3 or 12 h. After the initial H_2O_2 treatment, FRDA cells sustained relatively similar amounts of mtDNA damage compared to control fibroblasts, however, FRDA fibroblasts recovered more slowly than control cells as shown by the results of mtDNA damage assays (Fig. 5A). Following 12 h of recovery from H_2O_2 treatment, amplification of mtDNA in control fibroblasts reached approximately 70% of the levels in untreated cells. In contrast, after the same length of recovery time in H_2O_2-treated FRDA cells, amplification of mtDNA reached approximately 50% of the level detected in untreated FRDA cells (Fig. 5A). We did not observe any effects on morphology or viability of control and FRDA fibroblasts after treatment with H_2O_2 (Fig. 5B). In summary, FRDA cells demonstrate slower kinetics in repairing oxidative mtDNA damage, which in combination with greater levels of nuclear and mitochondrial DNA damage insults detected in cells expressing low levels of *FXN*[19,35], may lead to the progressive accumulation of mtDNA damage.

DNA repair defect in FRDA cells

Increased mtDNA damage and delayed repair of oxidative damage observed in FRDA cells indicate a possible global

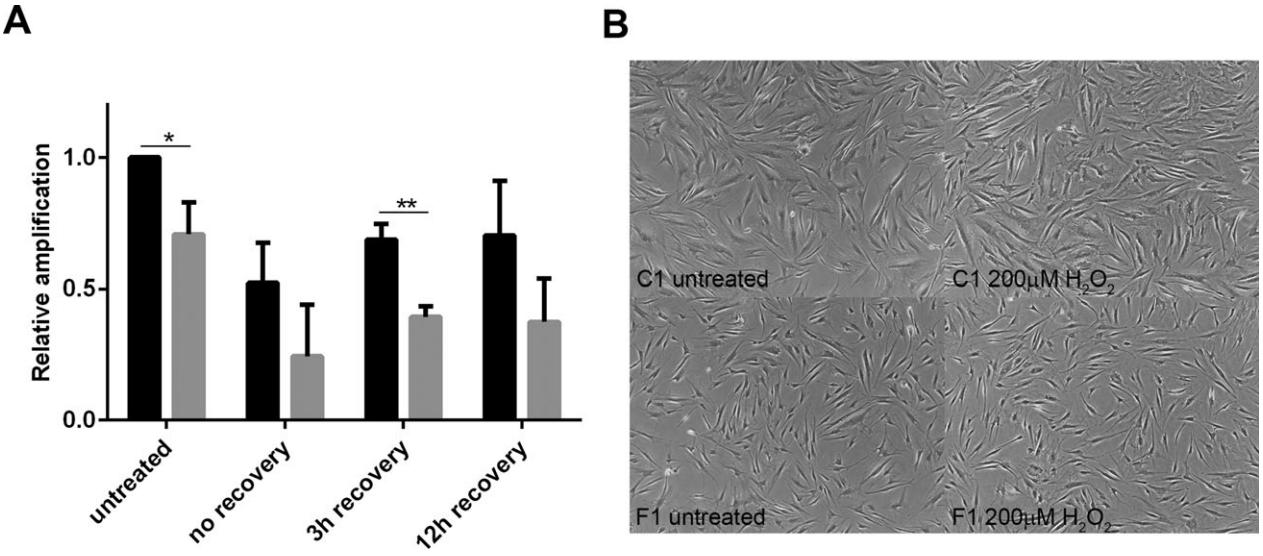

Figure 5. Repair of oxidative DNA damage is diminished in FRDA fibroblasts. (A) C1 and F1 cells were treated with 200 μmol/L H_2O_2 for 15 min and allowed to recover for 3 h or 12 h. Graph depicts results of mtDNA damage qPCR analysis. The average of three independent experiments is presented; *P = 0.014; **P = 0.002. (B) Representative images of fibroblasts before and after treatment with 200 μmol/L H_2O_2.

defect in mtDNA repair pathways. As BER is the predominant DNA repair system acting in mitochondria[36], we sought to determine the expression of all genes encoding DNA glycosylases functioning in mitochondria[37]. To compare comprehensively expression of these genes, we employed an RNA sequencing (RNA-seq) data set obtained using 18 FRDA and 17 control fibroblasts lines previously reported by our laboratory[30]. Of the 11 mammalian DNA glycosylases catalyzing the first step of removal of damaged bases, only *NTHL1* was significantly downregulated in FRDA cells (~60% of *NTHL1* mRNA detected in control cohort; Fig. 6A). The analyzed fibroblast lines included C1–C5 and F1–F5 used for mtDNA damage and sequencing studies described earlier. In addition, *NTHL1* expression highly correlated with *FXN* mRNA levels ($r = 0.73$, Fig. 6B), suggesting that deficiency of *FXN*, compounded by increased oxidative insult and insufficient levels of *NTHL1,* is responsible for the higher mtDNA mutation load in FRDA cells.

Discussion

While elevated mtDNA damage and increased ROS have been reported in FRDA cells, the potential effect of FXN deficiency on DNA mutagenesis and mitochondrial genome stability remains unknown. To elucidate the effect of *FXN* downregulation on mitochondrial DNA, we conducted comprehensive sequencing analyses of mtDNA in five FRDA and five control primary fibroblast lines. FRDA cells have an elevated mtDNA mutation frequency, which, if accumulated without repair, could be pathogenic in Friedreich's ataxia target cells. Additionally, shRNA-mediated depletion of *FXN* in control cells resulted in rapid accumulation of mtDNA damage indicating that a reduction of *FXN* levels is translated into defects in DNA metabolism and that adequate *FXN* expression may, in fact, protect the mitochondrial genome.

We identified more than 2300 residues in mtDNA that are more frequently mutated in FRDA cells than in controls. Of the most frequently mutated residues in FRDA cells, 14 were mutated 11–54-fold more often in FRDA cells than the background frequency determined in control cells. The mutations we found occurred uniformly throughout the mitochondrial genome, without any apparent enrichment in particular genes. It is important to consider that FRDA fibroblasts do not demonstrate any overt defect in cellular phenotype and are not the primary cell type affected in FRDA individuals, suggesting that increased mutation load in these cells is unlikely to affect the integrity of specific mitochondrial genes. On the other hand, high mtDNA mutation load could have more deleterious consequences on FRDA-affected cell types such as nonproliferating terminally differentiated neurons. Moreover, mitochondrial DNA mutations may represent an early event in FRDA neurodegeneration, accumulating over time to a critical threshold in postmitotic neurons, before triggering cell death. Similar patterns of numerous, widespread mtDNA mutations have also been associated with aging[38], indicating that the FRDA phenotype may be in part caused by accelerated mitochondrial aging.

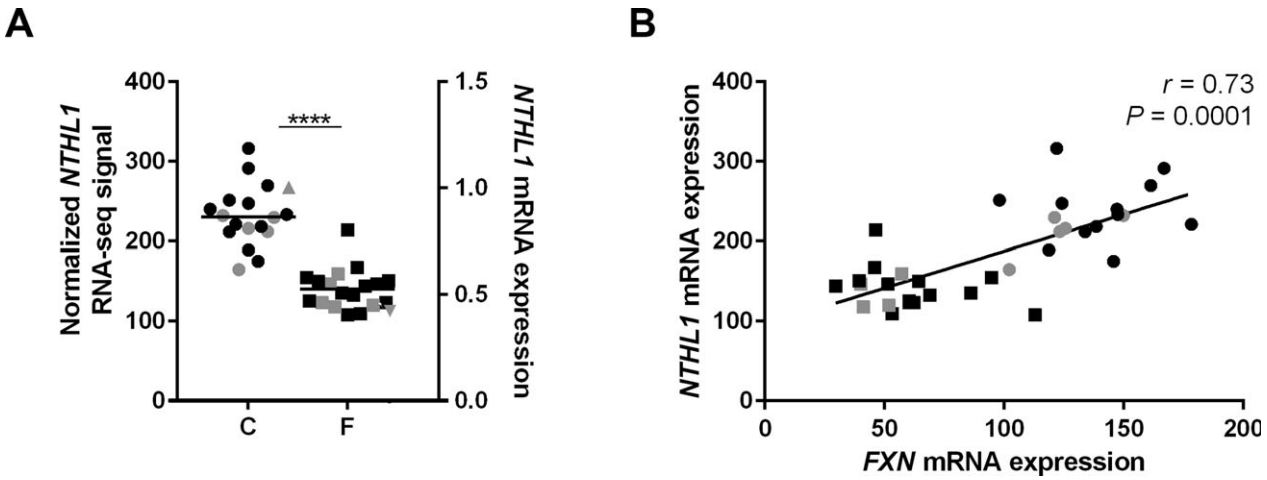

Figure 6. Downregulation of *NTHL1* expression in FRDA fibroblasts. (A) *NTHL1* expression was determined by RNA-seq[30] (control cohort-circles, FRDA cohort-squares) or by qRT-PCR (triangles; in the case where no RNA-seq analysis was available). Samples C1–C5 and F1–F5 used in mtDNA damage and frequency analyses are indicated in gray; ****$P = 0.0002$ and was calculated for RNA-seq samples only. (B) The Pearson correlation coefficient was determined for *FXN* mRNA and *NTHL1* mRNA expression in control and FRDA fibroblasts. Designations of symbols as described in A. Pearson's correlation coefficient (r) and statistical significance (P) values are indicated on the graph.

Overall, the higher number of transitions compared to transversions detected in all FRDA and control samples agrees with previous reports of general transition bias observed in human mitochondrial DNA[38]. As oxidative stress and increased ROS are implicated in FRDA origin and progression, we determined the frequency of specific mutations that may result from oxidative insult to mtDNA. Over 80 different products of ROS-induced DNA base damage are known, however, the most prevalent are 5-hydroxy-2′-deoxycytidine (5-OH-dC) and 8-oxo-7,8-dihydro-2′-deoxyguanosine (8-oxo-dG)[36,39]. Failure to repair these lesions leads to [C>T, G>A] transitions or [G>T, C>A] transversions, respectively. Our analyses demonstrated that [C>T, G>A] transitions were significantly enriched in mtDNA from FRDA cells rather than controls, indicating a specific increase in deoxycytidine oxidation and/or impaired repair pathways responsible for removal of these lesions.

Increased mutation load points toward an underlying misregulation of processes generating mutagenic metabolites, decreased fidelity of DNA replication or malfunction of repair systems responsible for error correction. Frataxin is required for the biosynthesis of ISCs that are important cofactors for several enzymes, many of which are critical for mitochondrial respiration, such as respiratory chain complexes I–III and mitochondrial aconitase. Decreased activity of these enzymes could result in mitochondrial dysfunction and elevated ROS production[40,41]. Moreover, ISCs are critical components of DNA repair proteins including DNA glycosylases NTHL1 and MutY DNA glycosylase (MUTYH), as well as replicative machinery proteins such as primase (PRIM2), DNA polymerase delta_1 (POLD1), and DNA helicases such as Fanconi anemia group J (FANCJ), regulator of telomere elongation (RTEL1) and DNA replication ATP-dependent helicase/nuclease DNA2 (DNA2)[42].

Our results demonstrate delayed recovery from peroxide-induced mtDNA damage in FRDA cells, suggesting reduced proficiency of DNA repair system(s). Comprehensive expression analysis of genes involved in BER, the main mtDNA repair pathway by which DNA lesions such as oxidized bases are removed[36], revealed that *NTHL1* is significantly decreased in FRDA fibroblasts compared to controls and correlates with expression of *FXN* mRNA. NTHL1 is a DNA glycosylase, active in the nucleus and mitochondria, responsible for repair of oxidized pyrimidines such as thymine glycol and 5-hydroxycytosine[36,43]. Depletion of this enzyme increased levels of [C>T, G>A] transitions, similar to the mutation class upregulated in FRDA fibroblasts[44]. In contrast, expression of *OGG1* (8-oxoguanine DNA glycosylase), the major glycosylase involved in the repair of 8-oxo-dG, was not affected in FRDA cells. No changes in expression of any additional BER genes were observed. These findings suggest that the elevated mutation load of FRDA mtDNA results from increased oxidative insult combined with reduced proficiency for the repair of certain DNA lesions. In agreement with our findings, decreased expression and enzymatic activity of *Nthl1* was previously shown in cardiac tissue isolated from *Fxn* conditional knockout mice[45]. Thus, reduced BER capacity may contribute to the development and progression of Friedreich's ataxia. Interestingly, DNA repair deficits have been associated with other forms of ataxia such as ataxia telangiectasia (AT), caused by mutations in ataxia telangiectasia-mutated (ATM) protein leading to deficits in double-strand break repair, as well as ataxia with oculomotor apraxia type 1 and 2 (AOA1, AOA2) and spinocerebellar ataxia with axonal neuropathy (SCAN1), caused by defects in aprataxin (APTX), senataxin (SETX), and tyrosyl-DNA-phosphodiesterase 1 (TDP1), respectively[46].

In the model proposed in Figure 7, we postulate that the pleiotropic effects of FXN deficiency on proteins and

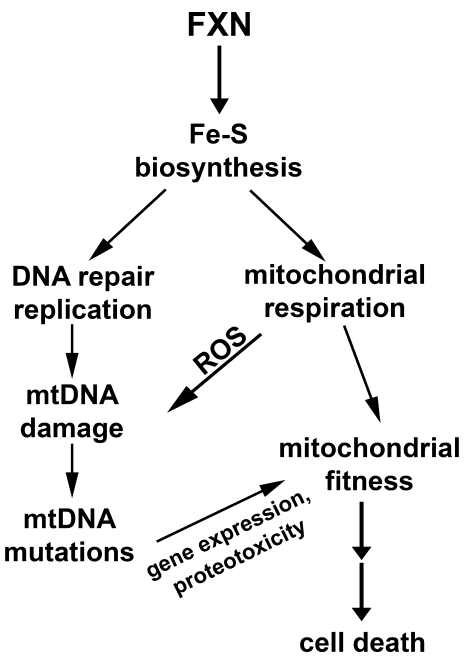

Figure 7. Proposed role of mtDNA damage and mutations in pathogenesis of FRDA. Impaired Fe–S cluster metabolism in *FXN*-deficient cells can alter DNA metabolism including replication and repair, causing an increase in mtDNA damage, and accelerating the formation of mtDNA mutations. Elevated mutation load can disturb mitochondrial gene expression. Further, reduced Fe–S cluster biosynthesis causes defects in mitochondrial respiration that may stimulate additional mtDNA damage via excessive reactive oxygen species (ROS) production. Both directly or indirectly, consequences of elevated mtDNA mutation load stemming from frataxin deficiency can reduce mitochondrial fitness. Insults accumulated over time may exceed a certain threshold of cellular tolerance initiating a cascade of events leading to the death of FRDA target cells.

processes dependent on ISCs lead to elevated DNA damage and mutation load by deregulation of oxidative metabolism in cells and impaired proficiency of DNA metabolism processes, such as repair and replication. Progressive malfunction of respiratory functions in FRDA cells may directly contribute to deterioration of mitochondrial functions as well as indirectly stimulate DNA mutagenesis by reduced control of ROS production[11,13,47,48]. Increased mutation burden of mtDNA can translate into aberrant expression of mitochondrial genes, especially if selected somatic mutations undergo clonal expansions, leading to potential respiratory chain dysfunction. Additionally, expression of mutation-containing mitochondrial genes can result in the production of aberrant, misfolded, and nonfunctional proteins. Pulse-chase experiments conducted in a mutator mouse model demonstrating increased frequency of widespread mtDNA mutations showed elevated protein turnover, providing evidence that translation of mutated mtDNA transcripts results in proteins that are misfolded and cannot be assembled correctly into respiratory complexes[49]. It is tempting to speculate that exceeding a certain threshold of mtDNA mutations, perhaps in combination with increased nuclear genome mutation burden, could overload protein clearance systems resulting in protein toxicity and cell death. Thus, a large body of evidence collected thus far by several different laboratories and in various model system indicates that mtDNA damage, mutations, as well as defects in DNA repair pathways can be an important modifier of FRDA progression contributing significantly to differences observed in clinical presentation of the disease. Analyses of mitochondrial DNA in patient tissues, especially obtained from cells primarily affected in FRDA will determine to what extent the stability of the mitochondrial genome contributes to the disease.

A widespread increase of mutations in mtDNA may be difficult to reverse, however, strategies aimed at reducing insults to the DNA, such us antioxidants targeting ROS, might in the long-term demonstrate therapeutic or preventive benefits. Additionally, mtDNA lesions could represent reliable disease biomarkers. In fact, stability of the mitochondrial genome and the extent of mtDNA mutations are intensively investigated as potential cancer biomarkers[50]. In Alzheimer's disease, the level of cell-free mtDNA has been measured as a novel preclinical biomarker with possible broader relevance to other neurodegenerative disorders[51]. Lack of appropriate biomarkers for FRDA hampers the development and evaluation of novel therapeutic strategies[52]. Precisely quantified mtDNA lesions are attractive candidates as surrogate end points to measure the efficacy of novel therapies. Many preclinical drug development programs in FRDA aim to elevate insufficient frataxin levels, reverse ROS accumulation, or inhibit neurodegeneration. Improvement in any of the above disease hallmarks is likely to result in measurable alleviation mtDNA mutations.

In summary, next-generation sequencing of FRDA mitochondrial genomes revealed a widespread increase in mutation load in patient fibroblasts. Although mtDNA damage alone can have profound consequences within the cell, low expression of FXN may also affect the nuclear genome as recent studies have demonstrated shortening of telomeres in cells derived from FRDA patients[53]. Importantly, mitochondrial ISC assembly machinery contributes to the biogenesis of both cytosolic and nuclear ISC-containing proteins. Therefore, it would be of interest to extend these studies into whole-genome analyses of FRDA samples including terminally differentiated neurons, glia, and cardiac cells (i.e., cell types in which the pathological changes are the most pronounced). BER deficiency could also affect the stability of GAA repeats and, combined with increased DNA damage, lead to progressive expansions in a tissue-specific fashion[54]. Taken together, the critical location of frataxin in the ISC biosynthesis pathway may lead to widespread genomic consequences that can translate to disease onset and progression.

Acknowledgments

The authors thank Dr. Jill Sergesketter Butler and Amanda Clark for critical comments and technical support, and Dr. Keith Giles for Control 3 primers.

Author Contributions

M. N. and A. D. B. conceived and designed experiments, analyzed and interpreted data, and wrote the manuscript. A. D. B. performed experiments and created figures A.K-J. conducted bioinformatic analyses. Y. L. performed experiments. D. R. L. provided materials. All authors critically revised the manuscript for important intellectual content and approved the final version of the manuscript.

Conflicts of Interest

The authors report no conflicts of interest.

References

1. Pandolfo M. Friedreich ataxia: The clinical picture. J Neurol 2009;256(Suppl 1):3–8.
2. Koeppen AH, Mazurkiewicz JE. Friedreich ataxia: neuropathology revised. J Neuropathol Exp Neurol 2013;72:78–90.

3. Campuzano V, Montermini L, Molto MD, et al. Friedreich's ataxia: autosomal recessive disease caused by an intronic GAA triplet repeat expansion. Science 1996;271:1423–1427.
4. Puccio H, Anheim M, Tranchant C. Pathophysiogical and therapeutic progress in Friedreich ataxia. Rev Neurol (Paris) 2014;170:355–365.
5. Lane DJ, Richardson DR. Frataxin, a molecule of mystery: trading stability for function in its iron-binding site. Biochem J 2010;426:e1–e3.
6. Rouault TA. Mammalian iron-sulphur proteins: novel insights into biogenesis and function. Nat Rev Mol Cell Biol 2015;16:45–55.
7. Paupe V, Dassa EP, Goncalves S, et al. Impaired nuclear Nrf2 translocation undermines the oxidative stress response in Friedreich ataxia. PLoS ONE 2009;4:e4253.
8. Seguin A, Sutak R, Bulteau AL, et al. Evidence that yeast frataxin is not an iron storage protein in vivo. Biochim Biophys Acta 2010;1802:531–538.
9. Sturm B, Bistrich U, Schranzhofer M, et al. Friedreich's ataxia, no changes in mitochondrial labile iron in human lymphoblasts and fibroblasts: a decrease in antioxidative capacity? J Biol Chem 2005;280:6701–6708.
10. Lodi R, Cooper JM, Bradley JL, et al. Deficit of in vivo mitochondrial ATP production in patients with Friedreich ataxia. Proc Natl Acad Sci USA 1999;96:11492–11495.
11. Bulteau AL, O'neill HA, Kennedy MC, et al. Frataxin acts as an iron chaperone protein to modulate mitochondrial aconitase activity. Science 2004;305:242–245.
12. Babcock M, De Silva D, Oaks R, et al. Regulation of mitochondrial iron accumulation by Yfh1p, a Putative Homolog of Frataxin. Science 1997;276:1709–1712.
13. Puccio H, Simon D, Cossee M, et al. Mouse models for Friedreich ataxia exhibit cardiomyopathy, sensory nerve defect and Fe-S enzyme deficiency followed by intramitochondrial iron deposits. Nat Genet 2001;27: 181–186.
14. Ramirez RL, Qian J, Santambrogio P, et al. Relation of cytosolic iron excess to cardiomyopathy of Friedreich's ataxia. Am J Cardiol 2012;110:1820–1827.
15. Cooke MS, Evans MD, Dizdaroglu M, Lunec J. Oxidative DNA damage: mechanisms, mutation, and disease. FASEB J 2003;17:1195–1214.
16. Li X, Fang P, Mai J, et al. Targeting mitochondrial reactive oxygen species as novel therapy for inflammatory diseases and cancers. J Hematol Oncol 2013;6:19.
17. Cha M-Y, Kim DK, Mook-Jung I. The role of mitochondrial DNA mutation on neurodegenerative diseases. Exp Mol Med 2015;47:e150.
18. Karthikeyan G, Santos JH, Graziewicz MA, et al. Reduction in frataxin causes progressive accumulation of mitochondrial damage. Hum Mol Genet 2003;12: 3331–3342.
19. Haugen AC, Di Prospero NA, Parker JS, et al. Altered gene expression and DNA damage in peripheral blood cells from Friedreich's ataxia patients: cellular model of pathology. PLoS Genet 2010;6:e1000812.
20. Heidari M, Houshmand M, Hosseinkhani S, et al. A novel mitochondrial heteroplasmic c13806a point mutation associated with Iranian Friedreich's ataxia. Cell Mol Neurobiol 2009;29:225–233.
21. Houshmand M, Panahi MS, Nafisi S, et al. Identification and sizing of GAA trinucleotide repeat expansion, investigation for D-loop variations and mitochondrial deletions in Iranian patients with Friedreich's ataxia. Mitochondrion 2006;6:87–93.
22. Singh I, Faruq M, Padma MV, et al. Investigation of mitochondrial DNA variations among Indian Friedreich's ataxia (FRDA) patients. Mitochondrion 2015;25:1–5.
23. Li Y, Polak U, Bhalla AD, et al. Excision of expanded gaa repeats alleviates the molecular phenotype of Friedreich's Ataxia. Mol Ther 2015;23:1055–1065.
24. Furda A, Santos JH, Meyer JN, Van Houten B. Quantitative PCR-based measurement of nuclear and mitochondrial DNA damage and repair in mammalian cells. Methods Mol Biol 2014;1105:419–437.
25. Bi R, Zhang AM, Zhang W, et al. The acquisition of an inheritable 50-bp deletion in the human mtDNA control region does not affect the mtDNA copy number in peripheral blood cells. Hum Mutat 2010;31:538–543.
26. Illumina. Human mtDNA genome for the illumina sequencing platform.2013.
27. Li H, Durbin R. Fast and accurate long-read alignment with burrows-wheeler transform. Bioinformatics 2010;26:589–595.
28. Mckenna A, Hanna M, Banks E, et al. The genome analysis toolkit: a mapreduce framework for analyzing next-generation DNA sequencing data. Genome Res 2010;20:1297–1303.
29. Anders S, Huber W. Differential expression analysis for sequence count data. Genome Biol 2010;11:R106.
30. Li Y, Lu Y, Polak U, et al. Expanded GAA repeats impede transcription elongation through the FXN gene and induce transcriptional silencing that is restricted to the FXN locus. Hum Mol Genet 2015;24:6932–6943.
31. Li Y, Polak U, Clark AD, et al. Establishment and maintenance of primary fibroblast repositories for rare diseases- Friedreich's ataxia example. Biopreserv Biobank 2016.
32. Andrews RM, Kubacka I, Chinnery PF, et al. Reanalysis and revision of the Cambridge reference sequence for human mitochondrial DNA. Nat Genet 1999;23:147.
33. Anderson S, Bankier AT, Barrell BG, et al. Sequence and organization of the human mitochondrial genome. Nature 1981;290:457–465.

34. Keller I, Bensasson D, Nichols RA. Transition-transversion bias is not universal: a counter example from grasshopper pseudogenes. PLoS Genet 2007;3:e22.
35. Thierbach R, Drewes G, Fusser M, et al. The Friedreich's ataxia protein frataxin modulates DNA base excision repair in prokaryotes and mammals. Biochem J 2010;432:165–172.
36. Alexeyev M, Shokolenko I, Wilson G, Ledoux S. The Maintenance of mitochondrial dna integrity—critical analysis and update. Cold Spring Harb Perspect Biol. 2013;5:a012641.
37. Prakash A, Doublié S. Base excision repair in the mitochondria. J Cell Biochem 2015;116:1490–1499.
38. Kennedy SR, Salk JJ, Schmitt MW, Loeb LA. Ultra-sensitive sequencing reveals an age-related increase in somatic mitochondrial mutations that are inconsistent with oxidative damage. PLoS Genet 2013;9:e1003794.
39. Poulsen HE. Oxidative DNA modifications. Exp Toxicol Pathol 2005;57(Suppl. 1):161–169.
40. Federico A, Cardaioli E, Da Pozzo P, et al. Mitochondria, oxidative stress and neurodegeneration. J Neurol Sci 2012;322:254–262.
41. Lenaz G. The mitochondrial production of reactive oxygen species: mechanisms and implications in human pathology. IUBMB Life 2001;52:159–164.
42. Fuss JO, Tsai C-L, Ishida JP, Tainer JA. Emerging critical roles of Fe–S clusters in DNA replication and repair. Biochim Biophys Acta 2015;1853:1253–1271.
43. Ikeda S, Biswas T, Roy R, et al. Purification and characterization of human NTH1, a Homolog of *Escherichia coli* Endonuclease III: direct identification of LYS-212 as the active nucleophilic residue. J Biol Chem 1998;273:21585–21593.
44. Weren RDA, Ligtenberg MJL, Kets CM, et al. A germline homozygous mutation in the base-excision repair gene NTHL1 causes adenomatous polyposis and colorectal cancer. Nat Genet 2015;47:668–671.
45. Martelli A, Wattenhofer-Donze M, Schmucker S, et al. Frataxin is essential for extramitochondrial Fe-S cluster proteins in mammalian tissues. Hum Mol Genet 2007;16:2651–2658.
46. Wells OS, El-Khamisy SF. Chapter 67 - autosomal recessive ataxias due to defects in dna repair a2- LeDoux, Mark S. Movement disorders 2nd ed. Boston: Academic Press, 2015.1033-41.
47. Rotig A, De Lonlay P, Chretien D, et al. Aconitase and mitochondrial iron-sulphur protein deficiency in Friedreich ataxia. Nat Genet 1997;17:215–217.
48. Carletti B, Piermarini E, Tozzi G, et al. Frataxin silencing inactivates mitochondrial Complex I in NSC34 motoneuronal cells and alters glutathione homeostasis. Int J Mol Sci 2014;15:5789–5806.
49. Edgar D, Shabalina I, Camara Y, et al. Random point mutations with major effects on protein-coding genes are the driving force behind premature aging in mtDNA mutator mice. Cell Metab 2009;10:131–138.
50. He Y, Wu J, Dressman DC, et al. Heteroplasmic mitochondrial DNA mutations in normal and tumour cells. Nature 2010;464:610–614.
51. Podlesniy P, Figueiro-Silva J, Llado A, et al. Low cerebrospinal fluid concentration of mitochondrial DNA in preclinical alzheimer disease. Ann Neurol 2013;74: 655–668.
52. Henchcliffe C, Beal MF. Mitochondrial biology and oxidative stress in Parkinson disease pathogenesis. Nat Clin Pract Neurol 2008;4:600–609.
53. Castaldo I, Vergara P, Pinelli M, et al. Can telomere shortening in human peripheral blood leukocytes serve as a disease biomarker of Friedreich's ataxia? Antioxid Redox Signal 2013;18:1303–1306.
54. McMurray CT. Mechanisms of trinucleotide repeat instability during human development. Nat Rev Genet 2010;11:786–799.

Supporting Information

Additional Supporting Information may be found online in the supporting information tab for this article:

Table S1. DEseq mismatch counts for C1–C5 and F1–F5.
Table S2. Library size factor normalized mutation frequency for C1–C5 and F1–F5.

